JOURNAL OF PLANKTON RESEARCH | VOLUME 32 | NUMBER 7 | PAGES 1023–1037 | 2010

Seasonal–spatial variation and remote sensing of phytoplankton absorption in Lake Taihu, a large eutrophic and shallow lake in China

YUNLIN ZHANG [1]*, LONGQING FENG [2], JUNSHENG LI [3], LIANCONG LUO [1], YAN YIN [1], MINGLIANG LIU [1] AND YUNLIANG LI [1]

[1]TAIHU LAKE LABORATORY ECOSYSTEM RESEARCH STATION, STATE KEY LABORATORY OF LAKE SCIENCE AND ENVIRONMENT, NANJING INSTITUTE OF GEOGRAPHY AND LIMNOLOGY, CHINESE ACADEMY OF SCIENCES, NANJING 210008, CHINA, [2]COLLEGE OF RESOURCES AND ENVIRONMENTAL SCIENCES, NANJING AGRICULTURAL UNIVERSITY, NANJING 210095, CHINA AND [3]EARTH OBSERVATION AND DIGITAL EARTH SCIENCE CENTER, CHINESE ACADEMY OF SCIENCES, BEIJING 100080, CHINA

*CORRESPONDING AUTHOR: ylzhang@niglas.ac.cn

Received October 24, 2009; accepted in principle March 10, 2010; accepted for publication March 15, 2010

Corresponding editor: William K.W. Li

Shallow water, strong sediment resuspension, complex river inputs and frequent cyanobacterial blooms characterize the waters of Lake Taihu. In such shallow, eutrophic lakes, the remote sensing of phycocyanin (PC), a characteristic pigment of cyanobacteria, is dependent on the estimation precision of phytoplankton absorption. For Lake Taihu, we monitored the seasonal–spatial variation of phytoplankton absorption, and a three-band model was calibrated and validated to estimate phytoplankton absorption ($a_{ph}(665)$) from a dataset of the spatial and temporal patterns of the bio-optical properties collected, during five cruises in January (winter), April (spring), July (summer), and October (autumn) in 2006 to 2007. Two distinct situations prevailed; in winter tripton strongly predominated over particulate matter, and in spring-summer-autumn phytoplankton made an important contribution. In winter, meteorology mainly determined the bio-optical properties of the water column, whereas in the spring-summer-autumn the biological activity was an additional active factor. The three-band remote sensing model $[R_{rs}^{-1}(673) - R_{rs}^{-1}(698)] \times R_{rs}(731)$ (R_{rs}: remote sensing reflectance) of $a_{ph}(665)$ was calibrated and validated, and its performance was compared and assessed with the published band-ratio method. With the three-band model, the root mean square error and mean relative error were 0.150 m^{-1} (50.5% accounting for the mean value) and 45.7% respectively; with the published band-ratio method, the values were 0.290 m^{-1} (97.3% accounting for the mean value) and 213.0% respectively, based on an independent validation dataset. Furthermore, the three-band and band-ratio models worked well in estimating phytoplankton absorption with simulated MERIS bands data with higher precision for the three-band model in Lake Taihu. The result showed that the three-band model was superior to the published band-ratio method, and thus the former can be used to improve the estimation precision of remote sensing of PC.

KEYWORDS: Lake Taihu; phycocyanin; phytoplankton absorption; remote sensing reflectance; three-band model

doi:10.1093/plankt/fbq039, available online at www.plankt.oxfordjournals.org. Advance Access publication April 9, 2010

INTRODUCTION

Aerial and satellite remote sensing provide more extensive temporal-spatial information about water quality and the extent of cyanobacterial blooms than does conventional monitoring in some coastal and lake waters (Gons, 1999, 2008; Simis *et al.*, 2005; Kutser *et al.*, 2006; Gitelson *et al.*, 2007). Color remote sensing is based on relationships between remote sensing reflectance and inherent optical properties (IOPs), total absorption, and backscattering coefficients (Kirk, 1994). The accurate application of this technique in lakes requires calibration, validation, and study of the IOPs at regional and seasonal scales.

During the last decade, the spectral absorption, spatial and seasonal variations of chromophoric dissolved organic matter (CDOM) have been widely studied. Considerable attention has been given to the spectral absorption and specific absorption of phytoplankton because the dynamics of these two variables are important for light attenuation and primary production in many productive areas of the oceans and inland waters (Allali *et al.*, 1997; Laurion *et al.*, 2000; Stedmon *et al.*, 2000; Simis *et al.*, 2005; Vähätalo *et al.*, 2005; Giardino *et al.*, 2007). In some cases, phytoplankton absorption may be the main contributor to the overall absorption in ocean, coastal, and lake waters, especially in the algal growth season (Babin *et al.*, 2003; Binding *et al.*, 2008). The absorption by phytoplankton depends on its growth and pigment composition, both of which can vary seasonally and spatially.

Chlorophyll *a* (Chl*a*) and phytoplankton biomass are the common parameters retrieved from color remote sensing in the oceans. However, increasing eutrophication and harmful blooms of toxic cyanobacteria in inland and coastal waters also require frequent and rapid monitoring of phycocyanin (PC, which is characteristic of cyanobacteria, for inland water quality management by remote sensing in response to eutrophication).

Estimates of PC concentration have often used the semi-empirical band-ratio algorithm of PC developed by Simis *et al.* (Simis *et al.*, 2005, 2007) for the band configuration of the Medium Resolution Imaging Spectrometer (MERIS), using MERIS channels 6, 7, 9 and 12 centered at 620, 665, 709 and 779 nm (Randolph *et al.*, 2008; Ruiz-Verdú *et al.*, 2008). Absorption in the 620 and 665 nm bands is assumed to be dominated by water and phytoplankton pigments (PC and Chl*a* at 620 nm, and Chl*a* alone at 665 nm), while the absorption in the 709 and 779 nm bands is assumed to be dominated by water alone. A spectrally neutral backscattering coefficient is derived from the 779 nm band, through inversion of a commonly used relationship between inherent optical properties and reflectance (Gordon *et al.*, 1975), as described in detail in Gons *et al.* (Gons *et al.*, 2005):

$$b_b(779) = \frac{1.61R_{rs}(779)}{0.082 - 0.6R_{rs}(779)} \quad (1)$$

Absorption coefficients in the 620 and 665 nm bands are then retrieved from the same reflectance model, through a ratio of the 709 nm band over each of the red bands (the band-ratio method). The absorption by PC at 620 nm is finally obtained after correcting for absorption by Chl*a* in the same band, proportional to the Chl*a* absorption coefficient derived at 665 nm. The detailed procedure is given and the algorithm equation was as follows (Gons, 1999; Gons *et al.*, 2005; Simis *et al.*, 2005, 2007):

$$a_{ph}(665) = 1.47 \times \left[\frac{R_{rs}(709)}{R_{rs}(665)} \times (0.727 + b_b) - b_b - 0.401\right] \quad (2)$$

$$PC = 170 \times \left\{\left[\frac{R_{rs}(709)}{R_{rs}(620)} \times (0.727 + b_b) - b_b - 0.281\right] - 0.24a_{ph}(665)\right\} \quad (3)$$

where $a_{ph}(665)$ was phytoplankton absorption coefficient at 665 nm; $R_{rs}(709)$ and $R_{rs}(665)$ were the remote sensing reflectance at 709 and 665 nm, respectively; PC was the PC concentration ($\mu g\ L^{-1}$); and b_b was the backscattering coefficient equal to $b_b(779)$ (m^{-1}). Equations (2) and (3) showed that the remote sensing of PC was dependent on the remote sensing precision of $a_{ph}(665)$. Therefore, accurate retrieval of phytoplankton was vital for PC estimation and harmful cyanobacterial blooms assessment.

The objectives of the present study were: (i) to quantify the concentrations and bio-optical properties (phytoplankton absorption and remote sensing reflectance) of optically active substances on seasonal (winter, spring, summer and autumn) and spatial scales (different lake regions), and (ii) to test the three-band model for phytoplankton absorption estimation, and compare the precision with the published band-ratio method given above in equation (2) (Simis *et al.*, 2007).

METHOD

Study site and sampling schedule

Optical measurements were made, and water samples were collected, at the surface (50 cm) along four transects

comprising 50 sites in different regions of Lake Taihu. The four transects were as follows (Fig. 1): transect 1, sites 1–16, followed a semi-circular route around Meiliang Bay in the north; transect 2, sites 17–29, originated in Gonghu Bay and extended southwest across the lake centre; transect 3, sites 30–40, originated in Guanghu Bay and extended southwest across the lake centre; transect 4, sites 41–50, originated in Xukou Bay and extended southwest across the lake south of Xishan Island.

Measurements and water samples were taken at 50 sites on five seasonal cruises: winter (7–9 January 2006, and 7–9 January 2007), spring (25–27 April 2007), summer (29 July–1 August 2006) and autumn (12–15 October 2006).

Wind speed data were obtained from the automatic weather station of the Taihu Laboratory for Lake Ecosystem Research (TLLER), Chinese Academy of Sciences, located at 31°25.42′, 120°12.57′ in the littoral of Meiliang Bay, in the north of the lake (Fig. 1). The wind speed ($m\,s^{-1}$) was the speed averaged over 10 min.

Optically active substances

Water samples for Chl*a* and phaeophytin-*a* (P*a*) (100–500 mL, according to the amount of phytoplankton) were filtered on Whatman GF/C filters. The Chl*a* and P*a* were extracted with ethanol (90%) at 80°C, and analyzed spectrophotometrically (using a Shimadzu UV-2401PC UV-Vis spectrophotometer) at 750 and 665 nm with correction for phaeophytin-*a* (Simis *et al.*, 2005).

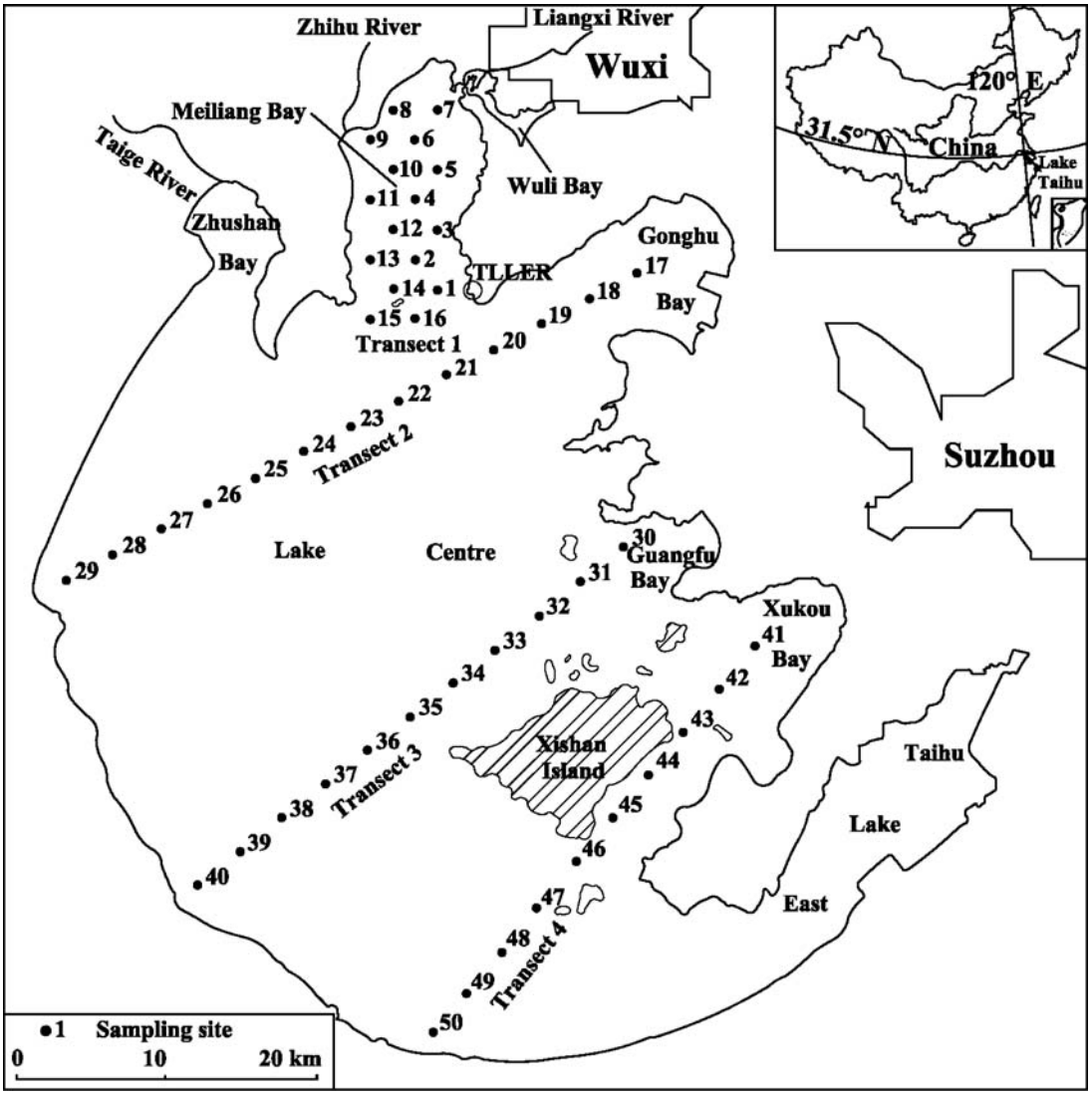

Fig. 1. Transects and sampling sites for bio-optical properties of water in Lake Taihu, China, in 2006 and 2007.

Total suspended matter (TSM) was filtered from water samples (100–500 mL, according to the amount of particles) using Whatman GF/C filters that had been pre-combusted at 450°C for 4 h; the filters were then dried at 105°C for 4 h, and weighed using an electrobalance with the accuracy of 10^{-5} g. Next, the filters were re-combusted at 450°C for 4 h and re-weighed to obtain inorganic suspended matter (ISM). Organic suspended matter was obtained by subtraction of ISM from TSM.

In order to determine the dry weight of tripton relative to the dry weight of total particles, the dominant species of *Microcystis* spp. and *Scenedesmus* spp. in Lake Taihu were cultured in the laboratory to measure their dry weight, Chl*a* and P*a* concentrations in different growth periods. Surface algal bloom samples were collected during calm weather, and cleaned using distilled water to obtain relatively pure phytoplankton (excluding tripton). Then the sample was put in darkness. Every 3 days during the 33-day experiment, a sample was collected to measure the dry weight, Chl*a* and P*a* concentrations. The following simple linear equation described the relationship between the dry weight of phytoplankton and the sum of Chl*a* and P*a* concentrations:

$$C_{\text{phytoplankton}} = 0.09 C_{\text{Chl}a+\text{P}a} \quad (r^2 = 0.98, n = 31, P < 0.001) \tag{4}$$

where $C_{\text{phytoplankton}}$ is the dry weight of phytoplankton, and $C_{\text{Chl}a+\text{P}a}$ is the sum of Chl*a* and P*a* concentrations. The concentration of tripton (C_{Tripton}) was obtained from the difference of TSM (C_{TSM}) and phytoplankton ($C_{\text{phytoplankton}}$) dry weights.

Measurement of remote sensing reflectance and inherent optical properties

Downwelling radiance and upwelling total radiance measurements were made with an ASD field spectrometer (Analytical Devices, Inc., Boulder, CO, USA) with a spectral response of 350–1050 nm, a spectral resolution of 3 nm and a sampling interval of 1 nm. The "above water method" was used to measure water surface spectra (Tang *et al.*, 2004). The detailed measurement procedure was as follows.

An optical fiber was positioned at nadir on a mount extending ~1 m away from the boat, to reduce the influence of reflectance from the vessel on collected spectra. The radiance spectra from the reference panel ($L_p(\lambda, 0^+)$), water ($L_{sw}(\lambda, 0^+)$) and sky ($L_{sky}(\lambda)$) were measured approximately 0.3 m above the water surface under clear sky conditions. At each sampling site, the spectra were measured 10 times to optimize the signal-to-noise ratio, and thus reduce the error of *in situ* measurements. Each spectrum was sampled 90° azimuthally from the sun, and at a nadir viewing angle of 40°, to avoid the interference of the ship with the water surface and the influence of direct sunlight. The water-leaving radiance $L_w(\lambda, 0^+)$ can be derived from the following equation:

$$L_w(\lambda, 0^+) = L_{sw}(\lambda, 0^+) - r_{sky} \cdot L_{sky}(\lambda) \tag{5}$$

where $L_{sw}(\lambda, 0^+)$ is the upwelling radiance from water, and $L_{sky}(\lambda)$ is the sky radiance measured at the same azimuth angle and at 40° zenith angle. The r_{sky} is the spectral reflectance of skylight at the air–water interface, which is dependent upon wind speed. Values of r_{sky} ranged from 0.022 in calm weather to 0.025 at wind speeds of up to 5 m s^{-1} (Tang *et al.*, 2004). A constant value of 0.0245 was used in this study.

The incident downwelling irradiance $E_d(\lambda, 0^+)$ was determined by measurement of the radiance of the Lambertian reference panel $L_p(\lambda, 0^+)$ as follows:

$$E_d(\lambda, 0^+) = \frac{\pi L_p(\lambda, 0^+)}{\rho_p(\lambda)} \tag{6}$$

where $\rho_p(\lambda)$ is the reflectance of the reference panel that was accurately calibrated to 30%.

The remote sensing reflectance above the water surface $R_{rs}(\lambda, 0^+)$ was calculated as the ratio of water-leaving upwelling radiance $L_w(\lambda, 0^+)$ to incident downwelling irradiance $E_d(\lambda, 0^+)$. Some $R_{rs}(\lambda, 0^+)$ spectra were excluded from the data set at sites with a thick algal bloom or macrophytes. A set of 223 $R_{rs}(\lambda, 0^+)$ spectra was obtained in this study.

The total data set (223 samples) was randomly divided into two groups (calibration and validation datasets) across all seasons. The calibration data set contained two-thirds of the samples (149), and the validation data set contained one third of the samples (74).

The absorption coefficient of total particulate matter $a_p(\lambda)$ (including tripton and phytoplankton), tripton $a_d(\lambda)$ and phytoplankton $a_{ph}(\lambda)$ were determined by the quantitative filter technique (QFT) where methanol was used to partition the absorption of tripton and phytoplankton. Water samples were first filtered through a 47-mm-diameter Whatman 0.70 μm GF/F filter, and then re-filtered through a 25-mm-diameter 0.22 μm Millipore filter to measure CDOM absorption. The absorption coefficients of the three other components ($a_p(\lambda)$, $a_d(\lambda)$ and $a_{ph}(\lambda)$) were measured with a Shimadzu UV-2401PC UV-Vis spectrophotometer; the

detailed measurement process was described by Zhang *et al.* (Zhang *et al.*, 2007).

The ratio of phytoplankton absorption to Chl*a* concentration was defined as the specific absorption coefficients of phytoplankton $a^*_{ph}(\lambda)$:

$$a^*_{ph}(\lambda) = \frac{a_{ph}(\lambda)}{C_{Chla}} \quad (7)$$

where C_{Chla} is Chl*a* concentration.

The three-band model of $a_{ph}(665)$

The three-band reflectance model was originally developed to estimate pigment concentrations in terrestrial vegetation. Reciprocal remote sensing reflectance in the first spectral band (λ_1) should be most sensitive to Chl*a* concentration. $R_{rs}(\lambda_1)$ is also affected by absorption by tripton, CDOM and water, as well as backscattering by all particulate matter. The effect of absorption by tripton and CDOM, and backscattering, can be minimized by the use of a second spectral band, where $R_{rs}(\lambda_2)$ is minimally sensitive to absorption by phytoplankton, tripton and CDOM. A third spectral band, $R_{rs}(\lambda_3)$, is minimally affected by phytoplankton, tripton and CDOM, and thus the total absorption in this third band is a measure of the absorption by water. Based on these assumptions, the spectral ranges of the three bands are restricted to 660–690 nm, 700–750 nm and 730–760 nm, respectively.

Many results have shown that in coastal and lake waters, the three-band model gives a better estimate of Chl*a* than the band ratio (Dall'Olmo and Gitelson, 2005; Zimba and Gitelson, 2006; Gitelson *et al.*, 2007, 2008; Li *et al.*, 2008; Xu *et al.*, 2009).

Gitelson *et al.* (Gitelson *et al.*, 2008) pointed out that the band-ratio and three-band models are based on the assumption that optical parameters, such as the Chl*a*-specific absorption coefficient and the Chl*a* fluorescence quantum yield, remain constant. However, many studies have shown that the Chl*a*-specific absorption coefficient varied greatly in spectral shape and magnitude because of differences in phytoplankton community, cell size and pigment packages among sites (Prieur and Sathyendranath, 1981; Millán-Núñez *et al.*, 2004). Therefore, the assumption of a constant for Chl*a*-specific absorption is a significant source of uncertainty in models for Chl*a* remote estimation (Dall'Olmo and Gitelson, 2005, 2006; Xu *et al.*, 2009).

However, for phytoplankton absorption remote estimation using the three-band model, this limitation will be removed.

The three-band model of phytoplankton absorption $a_{ph}(665)$ was expressed as follows:

$$a_{ph}(665) = A \times [R_{rs}^{-1}(\lambda_1) - R_{rs}^{-1}(\lambda_2)] \times R_{rs}(\lambda_3) + B \quad (8)$$

where A and B are constants that are dependent on the specific inherent optical properties, and the three wavelengths have to be determined *a priori* or *a posteriori*. R_{rs} is the remote sensing reflectance.

In order to assess the precision using MERIS data to estimate phytoplankton absorption, the mean values of reflectance in MERIS spectral bands (channel 7: 660–670 nm, channel 9: 704–714 nm, channel 10: 750–758 nm) calculated and the central wavelength values (channel 7: 665 nm, channel 9: 709 nm, channel 10: 753 nm) were used to calibrate and validate the three-band model and the band-ratio method, and the model values were compared with measured phytoplankton absorption.

Data analysis

The three sites with extremely high Chl*a* concentrations (>500 μg L^{-1}) (site 40 in spring, sites 10 and 16 in autumn) were excluded from the data sets in this study.

Statistical analysis (mean value, linear and nonlinear fitting) were performed with SPSS 11.0 software (Statistical Program for Social Sciences). Differences in parameters between two groups were assessed with a paired *t*-test using a *P*-value of 0.05 to determine significance. Regression and correlation analyses were used to examine the relationships between variables using SPSS software. Significance levels are reported as no significance ($P > 0.05$) or significance ($P < 0.05$). The regression determination coefficient (r^2), the root mean square error (RMSE) and mean relative error (MRE) were used to evaluate the performance of the retrieval model. The parameters of RMSE and MRE were derived with equations as follows:

$$\mathrm{RMSE} = \sqrt{\frac{\sum_{i=1}^{n}(x_{Est,i} - x_{Obs,i})^2}{n}} \quad (9)$$

$$\mathrm{MRE} = \frac{\sum_{i=1}^{n} |x_{(Est,i} - x_{Obs,i})/x_{Obs,i}|}{n} \times 100\% \quad (10)$$

where $x_{Est,i}$ and $x_{Obs,i}$ are the estimated and measured values, respectively; n is the number of data points.

RESULTS AND DISCUSSION

Seasonal and spatial variations in optically active substance concentrations

The seasonal–spatial variations in the three optically active substances (tripton, Chl*a* and CDOM) concentrations including four seasonal cruises (excluding the cruise in January 2007) have been presented by Zhang *et al.* (Zhang *et al.*, 2009a). Here, we just present the basic general temporal–spatial trends and some new insights based on more investigation cruises and bio-optical properties parameters. The seasonal variations in optically active substance concentrations, and in the bio-optical properties parameters of the water in Lake Taihu, are given in Table I.

The mean ISM and tripton concentrations decreased from winter to spring, summer and autumn (Table I). There were also significant spatial variations in mean ISM and tripton concentrations, with significantly higher concentrations on transect 3 than on the other three transects in all four seasons (*t*-test, $P < 0.05$). Wind stress significantly affected the seasonal and spatial distribution of ISM and tripton. The mean ISM and tripton concentrations in each season corresponded with the 3-day mean wind speed before the cruise [6.1, 3.5, 3.4 and 1.8 m s^{-1} in winter (2006 and 2007), spring, summer and autumn, respectively], suggesting that sediment resuspension caused by wind speed controls ISM and tripton concentrations. High wind speeds of >6 m s^{-1} immediately before the January (2006 and 2007) cruise caused increased sediment re-suspension, resulting in high ISM and tripton concentrations. Low wind speeds of <2 m s^{-1} immediately before the autumn cruise resulted in the relatively low ISM and tripton concentrations (Fig. 2 and Table I).

Chl*a* concentration had a strong seasonal pattern (Table I). The lowest Chl*a* concentration was in winter (mean 14.7 ± 7.1 μg L^{-1}), which was significantly lower than the highest during the spring bloom in April 2007 (mean 59.3 ± 94.7 μg L^{-1}). During the summer and autumn blooms, Chl*a* concentrations decreased compared with the spring bloom. Spatially, the mean concentrations of Chl*a* on transects 1, 2 and 3 were significantly higher than those on transect 4 in all four seasons (*t*-test, $P < 0.001$), reflecting the serious eutrophication and algal blooms in the northern regions of Lake Taihu.

Table I: Seasonal variation in concentrations of optically active substances and inherent optical properties of water in Lake Taihu, China

		C_{ISM}, mg L^{-1}	C_{OSM}, mg L^{-1}	$C_{Tripton}$, mg L^{-1}	C_{Chla}, μg L^{-1}	$a_{CDOM}(440)$, m^{-1}	$a_{ph}(440)$, m^{-1}	$a^*_{ph}(440)$, m^2 mg^{-1}	$a_{ph}(665)$, m^{-1}	$a^*_{ph}(665)$, m^2 mg^{-1}
Winter	Min	6.7	4.5	9.2	4.9	0.32	0.09	0.0127	0.04	0.0050
	Max	262.0	25.1	281.7	34.0	2.36	0.65	0.0405	0.36	0.0199
	Med	96.9	13.1	109.5	12.9	0.88	0.26	0.0200	0.10	0.0090
	Mea	107.4	13.4	119.1	14.7	0.91	0.30	0.0211	0.14	0.0095
	SD	54.0	4.7	58.4	7.1	0.35	0.13	0.0051	0.08	0.0031
Spring	Min	9.9	4.9	14.4	4.9	0.35	0.11	0.0138	0.04	0.0049
	Max	82.2	92.5	129.0	448.9	1.52	32.50	0.0730	9.44	0.0229
	Med	28.4	9.2	39.0	22.2	0.69	0.52	0.0353	0.23	0.0115
	Mea	33.1	16.2	45.7	59.3	0.74	3.14	0.0377	1.01	0.0129
	SD	18.4	18.7	25.2	94.7	0.25	6.22	0.0157	1.86	0.0047
Summer	Min	8.7	3.6	11.8	4.8	0.27	0.17	0.0168	0.08	0.0084
	Max	80.9	69.2	94.1	360.7	1.52	11.87	0.0514	5.71	0.0186
	Med	32.1	13.3	42.0	31.6	0.68	0.92	0.0261	0.43	0.0133
	Mea	33.5	14.9	43.2	50.6	0.71	1.35	0.0279	0.69	0.0135
	SD	16.1	11.3	19.4	58.1	0.26	1.77	0.0077	0.89	0.0026
Autumn	Min	4.4	3.7	7.9	4.0	0.46	0.09	0.0094	0.03	0.0024
	Max	42.4	39.8	74.1	246.6	1.52	5.18	0.0406	2.49	0.0164
	Med	19.0	6.9	24.3	18.9	0.83	0.33	0.0183	0.11	0.0069
	Mea	18.7	9.0	26.0	35.7	0.84	0.64	0.0197	0.27	0.0072
	SD	8.9	6.3	12.8	46.9	0.20	0.90	0.0069	0.44	0.0029

The dates of the sampling cruises and number of samples were: winter, 7–9 January 2006 and 7–9 January 2007, 100; spring, 25–27 April, 49; summer, 28 July–1 August, 50; and autumn, 12–15 October, 48.

C_{ISM}, C_{OSM}, $C_{Tripton}$, C_{Chla}: concentrations of ISM, OSM, tripton and chlorophyll *a*, respectively. $a_{CDOM}(440)$: CDOM absorption coefficient at 440 nm. $a_{ph}(440)$, $a_{ph}(665)$: phytoplankton absorption coefficient at 440 nm and 665 nm. $a^*_{ph}(440)$ and $a^*_{ph}(665)$: Chl*a*-specific absorption coefficient at 440 and 665 nm.

The minimum, maximum, mean and standard deviation of tripton, Chl*a* and CDOM concentrations in spring, summer and autumn are cited from Zhang *et al.* (2009a).

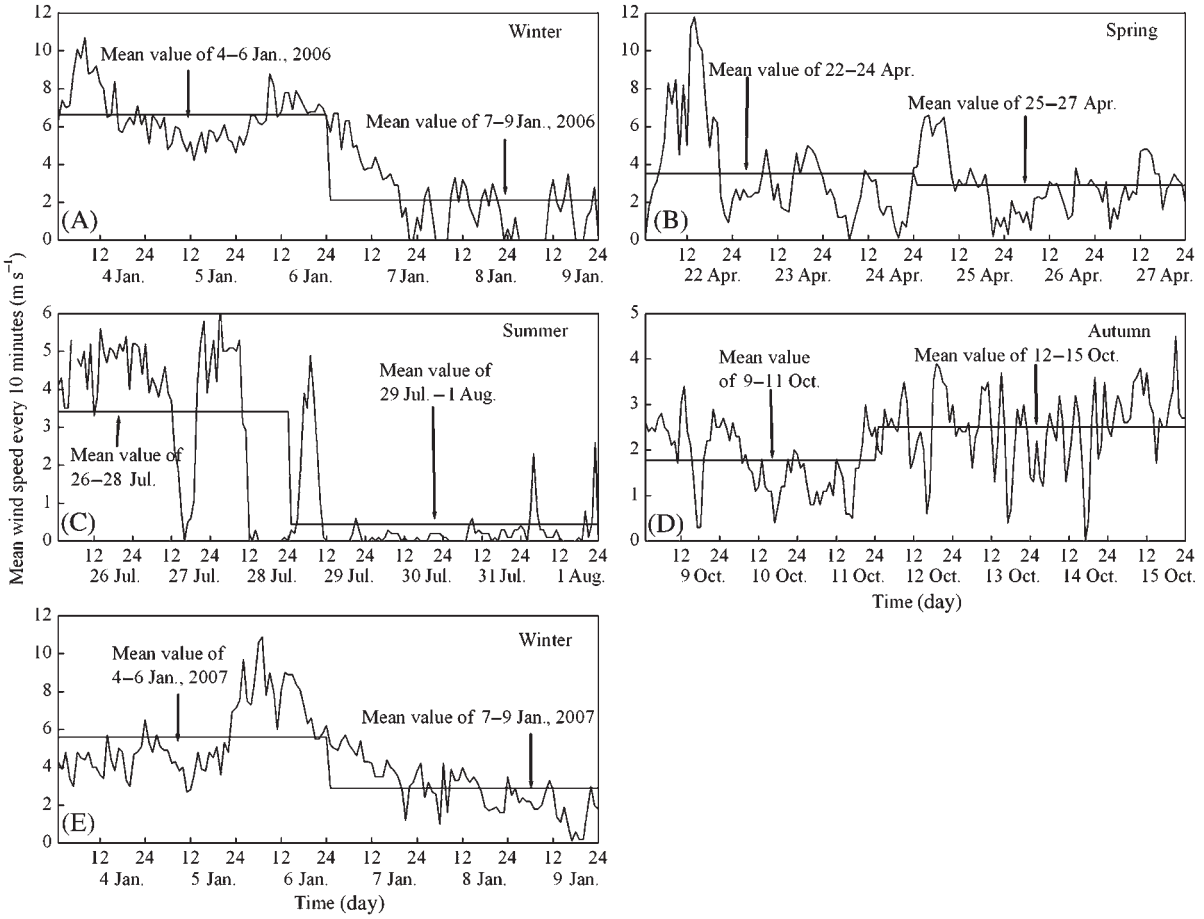

Fig. 2. Time series of wind speed in Lake Taihu, China, in 2006–2007. The horizontal line represents the means before and during cruises.

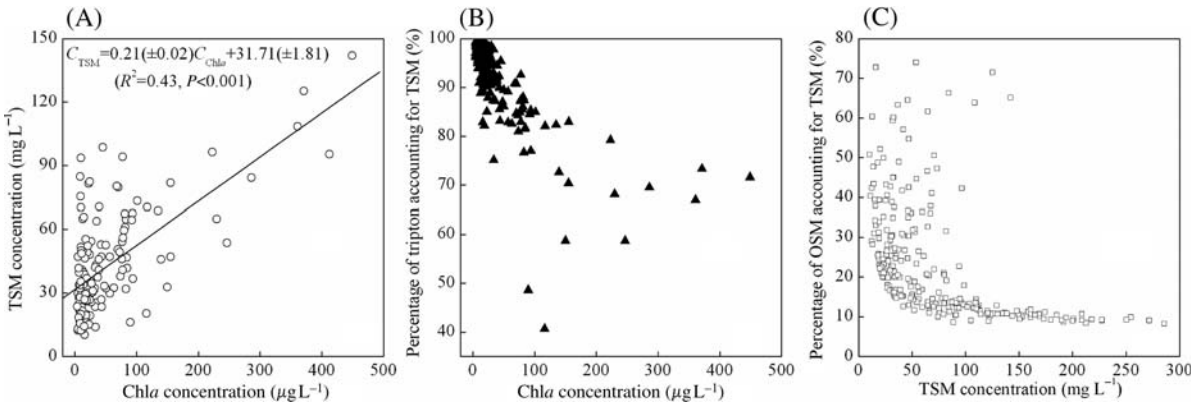

Fig. 3. Correlation between chlorophyll *a* (Chl*a*) and total suspended matter (TSM) concentrations in Lake Taihu during spring through autumn (excluding the data in winter) (**A**), percentage of tripton accounting for TSM as a function of Chl*a* concentration (**B**) and percentage of organic suspended matter (OSM) accounting for TSM as a function of TSM concentration (**C**).

In winter, there was no correlation between C_{TSM} and C_{Chla} ($P > 0.05$); however, in the three phytoplankton growth seasons, there was a significant positive correlation ($P < 0.001$) (Fig. 3A), which was very different from the winter period. This suggests that the interdependence between TSM and Chl*a* was quite strong in spring, summer and autumn due to the frequent algal blooms, which make a large contribution to TSM.

Actually, the percentages of pigment particles and organic matter increased when Chl*a* concentration increased; conversely, the percentages decreased when TSM increased (Fig. 3B and C). For stations in an algal bloom, TSM contained a large amount organic matter in addition to the inorganic matter.

The seasonal variability of the mean $a_{CDOM}(440)$ was characterized by a decrease from winter (January) to spring (April), a further slight decrease to summer (July and August), and then an increase in autumn (October) (Table I). Spatially, the mean CDOM absorption $a_{CDOM}(440)$ values along transects 1, 2, 3 and 4 were 1.06, 0.76, 0.73 and 0.63 m^{-1}, respectively, decreasing from Meiliang Bay to the northern lake region and to the southern lake region.

Phytoplankton absorption

The spectral absorption of phytoplankton and Chl*a*-specific absorption during different seasons are shown graphically in Fig. 4A–D and E–H, respectively, and the descriptive statistics are given in Table I.

There were large variations in the absorption coefficients of phytoplankton in different seasons and sites because of significant differences in pigment concentrations. The values for $a_{ph}(440)$ and $a_{ph}(665)$ were significantly lower in winter than in the other three seasons (*t*-test, $P < 0.001$), and the mean values of $a_{ph}(440)$ and $a_{ph}(665)$ on transects 1, 2 and 3 were significantly higher than those on transect 4 (*t*-test, $P < 0.001$) in all four seasons.

The seasonal and spatial variations of $a_{ph}(440)$ and $a_{ph}(665)$ were very similar to those of Chl*a* concentration, with increasing values from winter (January) to spring (April) and then decreasing values in summer (July and August) and in autumn (October) (Table I). The $a_{ph}(440)$ values of 0.09–32.50 m^{-1} and $a_{ph}(665)$ values of 0.03–9.44 m^{-1} corresponded with Chl*a* values of 4.0–448.9 $\mu g\ L^{-1}$

The absorption coefficients of phytoplankton were mainly affected by the composition of the population, and varied with changes in Chl*a* concentration. There were significant power correlations between $a_{ph}(440)$, $a_{ph}(665)$ and Chl*a* concentration ($a_{ph}(440) = 0.019C_{Chla}^{1.066}$, $r^2 = 0.87$, $P < 0.001$; $a_{ph}(665) = 0.0069C_{Chla}^{1.113}$, $r^2 = 0.87$, $P < 0.001$), which was consistent with the results observed in Case 1 and Case 2 waters (Bricaud *et al.*, 1998; Cao *et al.*, 2003). Values for $a_{ph}(440)$ and $a_{ph}(665)$ did not increase linearly, suggesting that specific absorption was not constant.

The ratio of $a_{ph}(400)$:$a_{ph}(440)$ reflects changes in the chlorophyll absorption peak at 440 nm, and should be <1. The model of Bricaud *et al.* (Bricaud *et al.*, 1995) produces a range for this ratio of 0.52 to 0.79 for Chl*a* concentrations from 0.01 to 50 $\mu g\ L^{-1}$. In the present

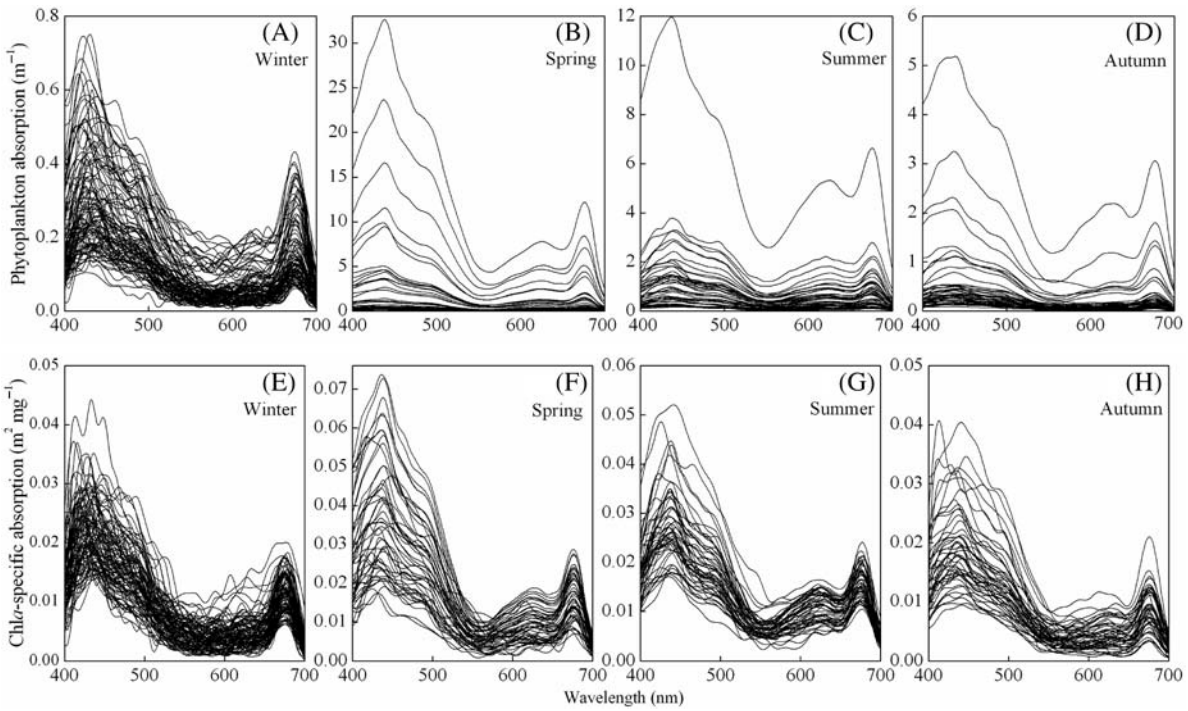

Fig. 4. Spectral variations of phytoplankton absorption (**A**–**D** for winter, spring, summer and autumn, respectively), and Chl*a*-specific absorption (**E**–**H** for winter, spring, summer and autumn, respectively) during different seasons in Lake Taihu, China.

study, the ratio $a_{ph}(400)$:$a_{ph}(440)$ ranged from 0.14 to 1.02; for most of our sites, the ratio of $a_{ph}(400)$:$a_{ph}(440)$ was less than 1. The mean was 0.67, which is within the range reported by Bricaud *et al.* (Bricaud *et al.*, 1995).

In the present study, the mean values of $a^*_{ph}(440)$ and $a^*_{ph}(665)$ in winter, spring, summer and autumn were 0.0211, 0.0377, 0.0279 and 0.0197 $m^2\,mg^{-1}$, and 0.0095, 0.0129, 0.0135 and 0.0072 $m^2\,mg^{-1}$ respectively. The value for $a^*_{ph}(440)$ was significantly higher in spring than in the other three seasons (*t*-test, $P < 0.001$), and for $a^*_{ph}(665)$, the values were significantly higher in spring and summer than in winter and autumn (*t*-test, $P < 0.001$).

There were no significant spatial differences for $a^*_{ph}(440)$ in the present study. The $a^*_{ph}(440)$ values we recorded in the eutrophic waters of Lake Taihu were less than the values observed in mesotrophic Lake Erie (Binding *et al.*, 2008), and in the ocean (Suzuki *et al.*, 1998; Sasaki *et al.*, 2001; Millán-Núñez *et al.*, 2004). The lower values in the eutrophic lake than in the oligotrophic oceans may reflect the predominance of blue green algae in Lake Taihu, whereas diatoms predominate in the oceans.

The Chl*a*-specific absorption coefficient is used to describe light absorption capability per unit of Chl*a*. This parameter is often considered to be relatively constant, averaging 0.016 $m^2\,mg^{-1}$ over 400–700 nm, when used in bio-optical modeling, in remote sensing of water color, underwater radiation and primary production. However, the Chl*a*-specific absorption coefficient actually varies locally and seasonally, and is affected by illumination and by the population structure of phytoplankton (Sosik and Mitchell, 1995; Lutz *et al.*, 1996; Stuart *et al.*, 2000). The measured Chl*a*-specific absorption coefficient $a^*_{ph}(440)$ lies within a range of 0.01–0.18 $m^2\,mg^{-1}$ and usually is higher in oligotrophic than in eutrophic waters (Bricaud *et al.*, 1995), as confirmed in the present study.

Spectral characteristics of remote sensing reflectance

The seasonal variation in remote sensing reflectance is shown in Fig. 5. The large variability in the concentration of the three optically active substances, and in their inherent optical properties, resulted in large seasonal and spatial variability in the magnitude of the remote sensing reflectance spectra. The reflectance spectra were highly variable at different sites and seasons.

In general, reflectance peaks occurred at around 560, 650, 700 and 810 nm (Fig. 5). Reflectance minima occurred at short wavelengths near 400 nm owing to the combined absorption by tripton, phytoplankton pigments and CDOM, and at longer wavelengths near 900 nm owing to high absorption by pure water. In turbid Lake Taihu, absorption by CDOM and tripton, and scattering by particulate matter, contributed most to reflectance in the range of 400–500 nm. A common characteristic of reflectance spectra in this range was low sensitivity to the variation of Chl*a* concentration. As a result, the blue-to-green ratio $R_{rs}(440)/R_{rs}(550)$ could not be used to estimate phytoplankton absorption in the waters of Lake Taihu ($a_{ph}(665) = -4.276R_{rs}(440)/R_{rs}(550) + 2.429$, $r^2 = 0.446$, $n = 223$, RMSE = 0.381 m^{-1}). Therefore, the difference in remote sensing reflectance at short wavelengths between different samples had no effect on estimation of phytoplankton absorption in the lake.

A peak in the green range near 550–570 nm (Fig. 5) was due to minimal absorption of all algal pigments (Fig. 4A–D); the scattering by ISM and phytoplankton cells controlled the magnitude of reflectance in this range. At around 675 nm, the reflectance minimum was due to phytoplankton absorption, especially at sites with high pigment concentration; however, reflectance in this range was strongly affected by tripton concentration and Chl*a* concentration, which decreased the correlation between $R_{rs}(675)$ and $a_{ph}(675)$. A local minimum around 625 nm was due to PC absorption. This pigment was present primarily in cyanobacteria; thus, a local reflectance minimum at 625 nm often has been used to monitor cyanobacterial blooms in eutrophic lakes (Simis *et al.*, 2005; Kutser *et al.*, 2006). The peak around 700 nm occurred in the spectral range of sharp decrease in Chl*a* absorption and increase of water absorption. Thus, the peak was due to minimal combined absorption of all pigments, materials and water. As Chl*a* concentration increased, the intersection of decreasing total absorption by pigments and materials with increasing water absorption shifts toward longer wavelength; therefore, the position of the peak shifted from 690 to 715 nm (Gitelson, 1992). The red shifting of the reflectance peak position near 700 nm with increasing Chl*a* concentration has also been observed in other productive turbid waters (Zimba and Gitelson, 2006; Gitelson *et al.*, 2007).

Some seasonal differences occurred in the remote sensing reflectance. During the phytoplankton growth season (spring–summer–autumn), the peaks near 560, 650 and 700 nm of the reflectance were more marked than in winter, especially for the peak near 700 nm caused by phytoplankton. For example, the maximal reflectance peak of two samples during the spring bloom (Fig. 5B) corresponded to the highest Chl*a* concentrations (229.7 and 222.8 $\mu g\,L^{-1}$, respectively). Reflectance was deleted from the data set for sites with Chl*a* concentrations of 371.0 and 448.9 $\mu g\,L^{-1}$ because the algal bloom (*Microcystis* spp.) covered the water

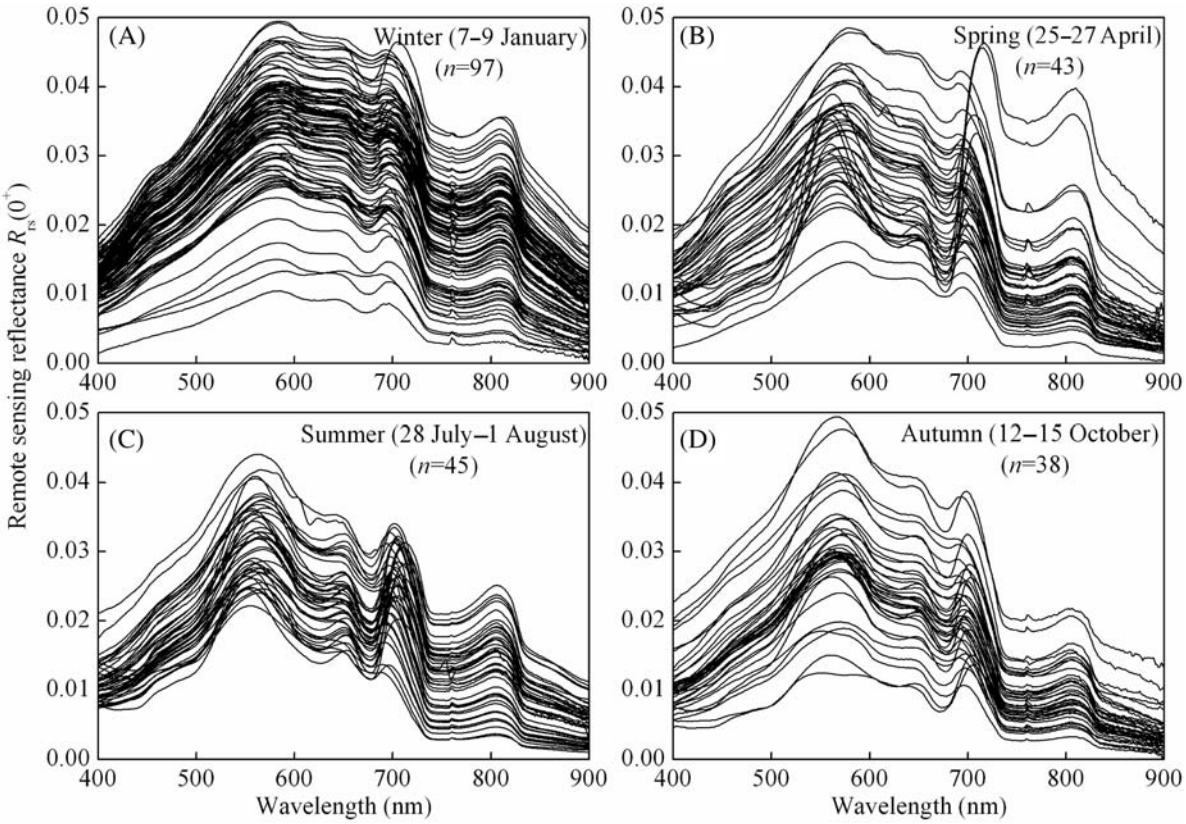

Fig. 5. Remote sensing reflectance in four different seasons during 2006–2007 in Lake Taihu, China. Each line represents a different site.

surface and affected the reflectance, which might not represent constituent concentrations. In winter, the peak near 560 nm appeared more like a shoulder (560–620 nm) due to the high backscattering caused by high ISM concentrations.

Spectra recorded in all four seasons in the extremely turbid Lake Taihu were different in magnitude and shape from the typical reflectance spectra measured in the slightly turbid Case 2 water by Gitelson *et al.* (Gitelson *et al.*, 2008). For example, in that study, the maximal reflectance was less than 0.03 in all five data sets, which was markedly lower than the maximal value measured in Lake Taihu, indicating the relatively low optically active substance concentration in their study. Furthermore, the peaks near 560, 650 and 700 nm were more marked in the Gitelson *et al.* (Gitelson *et al.*, 2008) study, suggesting a strong phytoplankton signal in their remote sensing reflectance.

The three-band model of $a_{ph}(665)$: calibration

The calibration data set contained 149 water samples, with $a_{ph}(665)$ ranging from 0.030 to 4.049 m^{-1} with a mean value of $0.319 \pm 0.538\ m^{-1}$. In order to find the best three bands by which to estimate $a_{ph}(665)$ in Lake Taihu, the combinations of any three wavelengths of λ_1 from 650 to 700 nm, λ_2 from 680 to 760 nm and λ_3 from 720 to 760 nm were used for correlation with $a_{ph}(665)$ by the use of the remote sensing reflectance according to the tuning procedure of Gitelson *et al.* (Gitelson *et al.*, 2007). The optimal band combination was judged by RMSE in the present study.

Xu *et al.* (Xu *et al.*, 2009) verified that the tuning procedure of optimal band positions for λ_1, λ_2 and λ_3 did not depend on the initial values of λ_1, λ_2 and λ_3. In the first step, we used initial positions for $\lambda_1^0 = 650$ nm and $\lambda_3^0 = 720$ nm in equation (8) to find the first approximation for position of $\lambda_2(\lambda_2^1)$. We regressed the model $[R_{rs}^{-1}(650) - R_{rs}^{-1}(\lambda_2)] \times R_{rs}(720)$ versus $a_{ph}(665)$ for the range of 680–760 nm, and found a minimal RMSE of $a_{ph}(665)$ estimation for λ_2 of around 698 nm (Fig. 6A). In the second step, we found a first approximation of λ_1^1, after fixing $\lambda_2^1 = 698$ nm and regressing the model $[R_{rs}^{-1}(\lambda_1) - R_{rs}^{-1}(698)] \times R_{rs}(730)$ versus $a_{ph}(665)$. The RMSE was minimal in a rather wide range of λ_1 around 673 nm (Fig. 6B). In the third step, we found a first approximation of λ_3 (λ_3^1), regressing the model $[R_{rs}^{-1}(673) - R_{rs}^{-1}(698)] \times R_{rs}(\lambda_3)$ versus $a_{ph}(665)$. The RMSE was minimal for $\lambda_3^1 = 731$ nm (Fig. 6C).

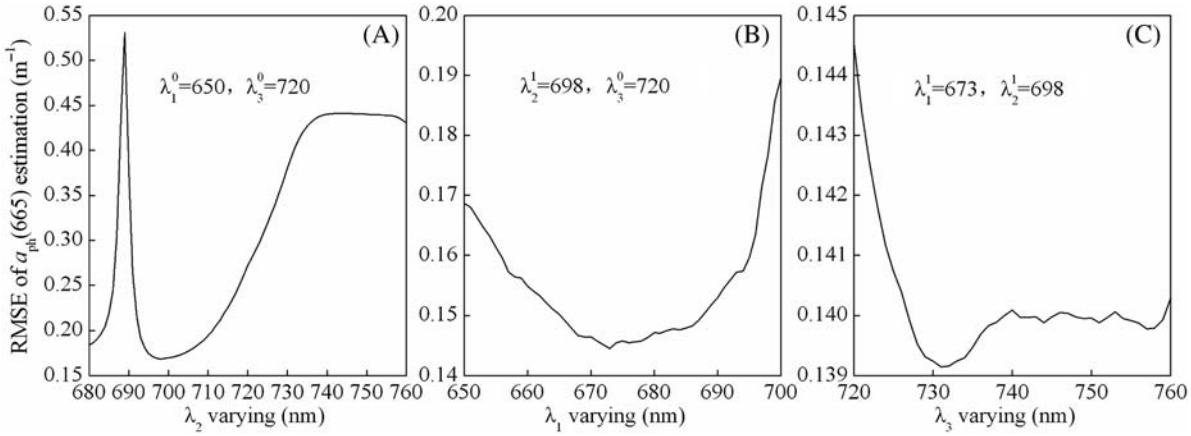

Fig. 6. RMSE error of $a_{ph}(665)$ estimation by the model equation (8). (**A**) Finding optimal λ_2^1 with initial λ_1^0 and λ_3^0; (**B**) finding optimal λ_1^1 with initial λ_3^0 and λ_1^1; (**C**) finding optimal $\lambda_2^{'}$ with λ_2^1 and λ_1^1. Optimal wavebands found as: $\lambda_1 = 673$ nm, $\lambda_2 = 698$ nm and $\lambda_3 = 731$ nm.

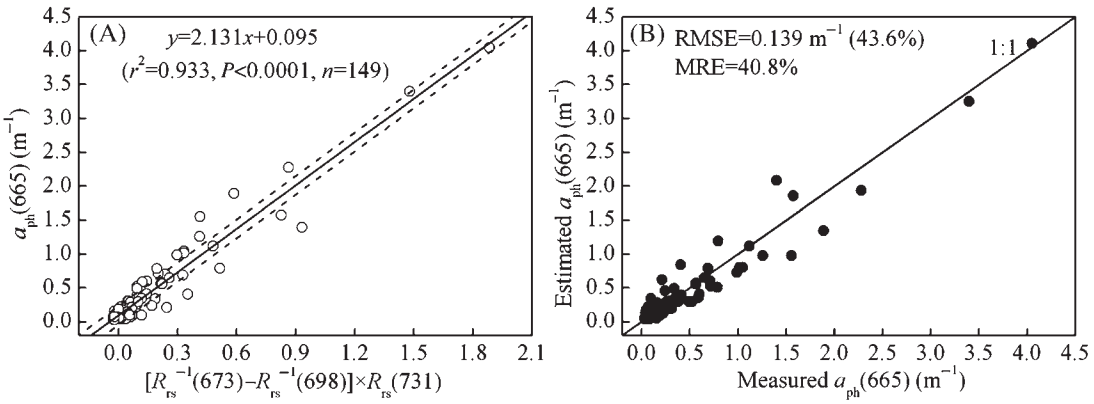

Fig. 7. (**A**) Retrieval model of phytoplankton absorption ($a_{ph}(665)$), and (**B**) comparison of measured and estimated values using the three-band model for water of Lake Taihu, China. The 43.6% in parentheses is the percentage of RMSE accounting for the mean $a_{ph}(665)$. In (A), the solid line indicates the linear fitting, and dotted lines indicate two RMSE of $a_{ph}(665)$ estimation.

Thus, we have found optimal spectral bands for $a_{ph}(665)$ estimation using the three-band combination $[R_{rs}^{-1}(673) - R_{rs}^{-1}(698)] \times R_{rs}(731)$, which were very similar to the optimal bands by Gitelson *et al.* (Gitelson *et al.*, 2007). The RMSE and the MRE were 0.139 m^{-1} (43.6% from the mean $a_{ph}(665)$) and 40.8% in the present study, respectively (Fig. 7). The measured and estimated values for C_{Chla} were distributed along the 1:1 line, indicating that the three-band reflectance model $[R_{rs}^{-1}(673) - R_{rs}^{-1}(698)] \times R_{rs}(731)$ could be used for the extremely turbid waters of Lake Taihu. Thus the three-band model for phytoplankton absorption estimation has the following form:

$$a_{ph}(665) = 2.131[R_{rs}^{-1}(673) - R_{rs}^{-1}(698)] \times R_{rs}(731) + 0.095 \quad (11)$$

The three chosen bands basically fall into the range of MERIS channels 8, 9, 10 (with centre wavelengths of 681, 709 and 754 nm, respectively), which would make it possible to estimate $a_{ph}(665)$ accurately using MERIS imagery. Considering that MERIS Channel 8 (681 nm) is close to chlorophyll fluorescence (683 nm), due to variability in quantum yield of chlorophyll fluorescence, and thus uncertainties in a_{ph} and chlorophyll *a* concentration retrieval, Dall'Olmo and Gitelson (Dall'Olmo and Gitelson, 2006) suggested that this band not be used. Therefore, Channel 7 (665 nm) is used as λ_1. The r^2, RMSE and MRE were 0.925, 0.146 m^{-1} and 50.1%, respectively (Fig. 8A), using the central bands of MERIS imagery $[R_{rs}^{-1}(665) - R_{rs}^{1}(709)] \times R_{rs}(754)$ based on the calibration data set, which gave high retrieval accuracy.

By using the spectral bands of MERIS channels 7 (660–670 nm), 9 (704–714 nm) and 10 (750–758 nm) $[R_{rs}^{-1}(660 - 670) - R_{rs}^{-1}(704 - 714)] \times R_{rs}(750 - 758)$, the three-band model was highly significant with r^2, RMSE and MRE of 0.925, 0.147 m^{-1} and 50.9%,

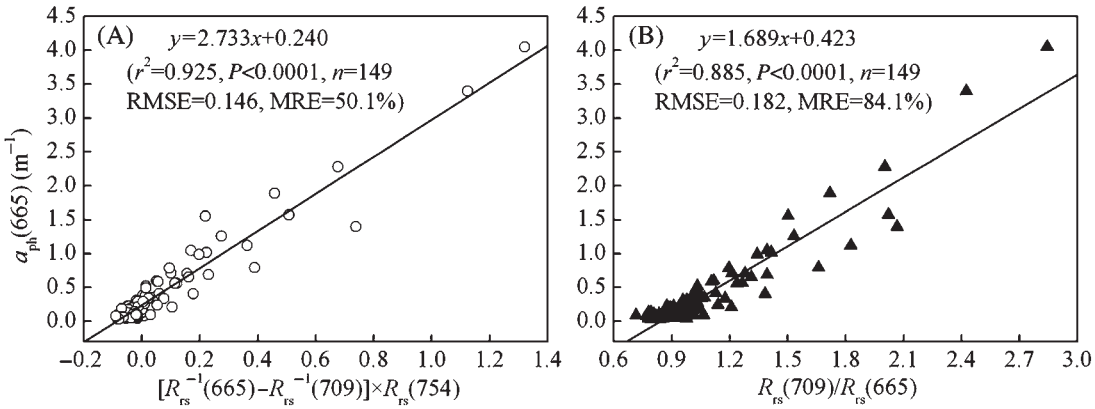

Fig. 8. Retrieval model of phytoplankton absorption ($a_{ph}(665)$) based on MERIS channels using (**A**) the three-band model, and (**B**) the band-ratio method.

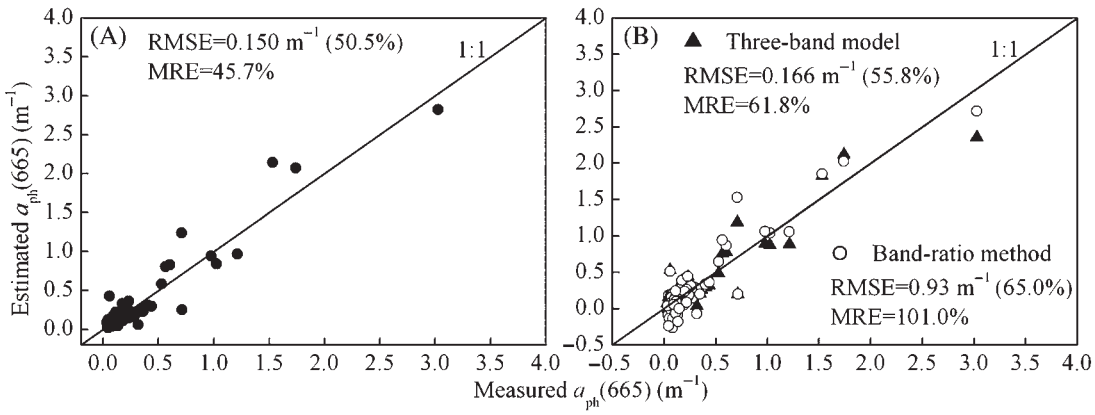

Fig. 9. Comparison of measured and estimated phytoplankton absorption ($a_{ph}(665)$) of the three-band model with "optimized" wavelength (Fig. 7) (**A**), the three-band model and the band-ratio method with simulated MERIS data (Fig. 8) (**B**) based on an independent data set from Lake Taihu, China. The 50.5, 55.8 and 65.0% in parentheses are the percentage of RMSE accounting for the mean $a_{ph}(665)$.

suggesting that MERIS data could be well used to estimate phytoplankton absorption. Recently, Moses *et al.* (Moses *et al.*, 2009) showed that the use of NIR-red model $R_{rs}(708)/R_{rs}(665)$ with MERIS spectral bands (Gitelson, 1992) resulted in more accurate estimates of chlorophyll *a* concentration than did a three-band model $[R_{rs}^{-1}(665) - R_{rs}^{-1}(709)] \times R_{rs}(753)$. However, this situation is not the case for Lake Taihu. The r^2, RMSE and MRE of the band-ratio method using MERIS band $R_{rs}(709)/R_{rs}(665)$ were only 0.885, 0.182 m^{-1} and 84.1%, respectively (Fig. 8B). Although the three-band model works better than the band-ratio method, we note that the band-ratio method is much more resistant to atmospheric effects.

The three-band model of $a_{ph}(665)$: validation

In order to further understand the applicability of the three-band model used to estimate phytoplankton absorption, we evaluated its performance by use of an independent validation data set. The value for $a_{ph}(665)$ ranged from 0.032 to 3.027 m^{-1} with a mean of 0.297 ± 0.455 m^{-1}, which fell into the range of $a_{ph}(665)$ used to calibrate the model. Comparisons of the measured and estimated $a_{ph}(665)$ using the calibrated three-band model (equation (11)) showed that these values were in close agreement with a highly significant linear relationship ($r^2 = 0.905$), with a slope of 1.014 and an intercept of 0.004, which were close to 1.0 and 0, respectively (Fig. 9A). Meanwhile, the three-band model $[R_{rs}^{-1}(665) - R_{rs}^{-1}(709)] \times R_{rs}(754)$ and the band-ratio method with simulated MERIS data showed high estimation precision with RMSE and MRE of 0.166 m^{-1} and 61.8% for the three-band model, and 0.193 m^{-1} and 101.0% for the band-ratio method based on the independent validation data set (Fig. 9B).

In order to assess the accuracy of retrieval models within the different $a_{ph}(665)$ level, Fig. 10 presented

MRE versus $a_{ph}(665)$. The performance (using MRE as the parameter) was significantly and negatively correlated with $a_{ph}(665)$ using the logarithm fitting of MRE versus $a_{ph}(665)$. For $a_{ph}(665)$ below 0.2 m^{-1}, there was a significant increase in the $a_{ph}(665)$ MRE. All MRE larger than 100% corresponded to $a_{ph}(665)$ of less than 0.2 m^{-1}. The high estimation of MRE for the low $a_{ph}(665)$ value resulted from two causes. First, the low $a_{ph}(665)$ resulted in the low contribution of phytoplankton to the total reflectance signal, which was concealed by the signal from other two optically active substances. The low $a_{ph}(665)$ generally corresponded to the high tripton concentration (Fig. 3). The increase of backscattering from tripton in the long wavelength would reduce the estimation precision of $a_{ph}(665)$. Secondly, phytoplankton absorption measurements also would increase the potential error for the low $a_{ph}(665)$ but high tripton concentration. The previous study (Zhang *et al.*, 2009b) showed that accurate and effective partition of the phytoplankton absorption spectra remained a considerable challenge when using experimental and numerical methods in turbid Case 2 waters with a low ratio of Chl*a*:TSM.

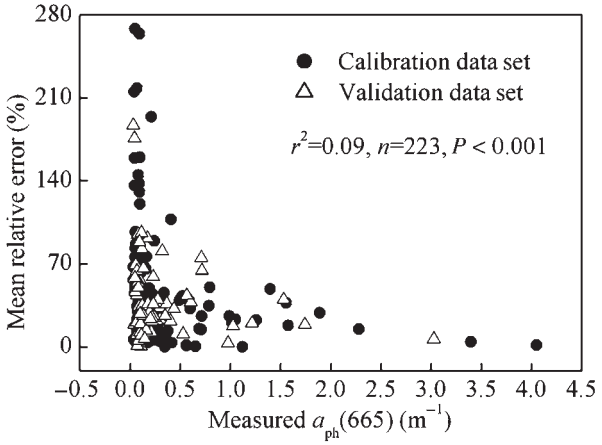

Fig. 10. The mean relative error of $a_{ph}(665)$ estimation plotted versus measured $a_{ph}(665)$. Determination coefficient and significant level are obtained from the logarithm fitting of MRE versus $a_{ph}(665)$.

Comparison of the three-band model with Simis *et al.* (2007) method

The measured and estimated values of $a_{ph}(665)$ using the three-band model with an independent data set, and the method of Simis *et al.* (Simis *et al.*, 2007) with calibration and validation data sets, are shown in Figs 9 and 11, respectively. The accuracy yielded by the three-band algorithm was better than that yielded by the algorithm of Simis *et al.* (Simis *et al.*, 2007). The RMSE of $a_{ph}(665)$ estimation by the three-band algorithm was 0.150 m^{-1}, as opposed to the RMSE of 0.290 m^{-1} from the algorithm of Simis *et al.* (Simis *et al.*, 2007) for the validation data set (Figs 9 and 11); these values were significantly different (*t*-test, $P < 0.001$). Although the three-band algorithm and the algorithm by Simis *et al.* (Simis *et al.*, 2007) are both adapted for MERIS spectral bands, there was significant and systematic overestimation of $a_{ph}(665)$ using the algorithm by Simis *et al.* (Simis *et al.*, 2007) for most stations in Lake Taihu. A possible reason for the poor performance of the Simis *et al.* (Simis *et al.*, 2007) algorithm was its use of a band at 778 nm to eliminate the backscatter effect, where the noise of radiometers used in the Dall'Olmo and Gitelson (Dall'Olmo and Gitelson, 2005) study was significant.

Combining the three-band algorithm of $a_{ph}(665)$ and the PC algorithm of Simis *et al.* (Simis *et al.*, 2007), an improved PC estimation model would provide more

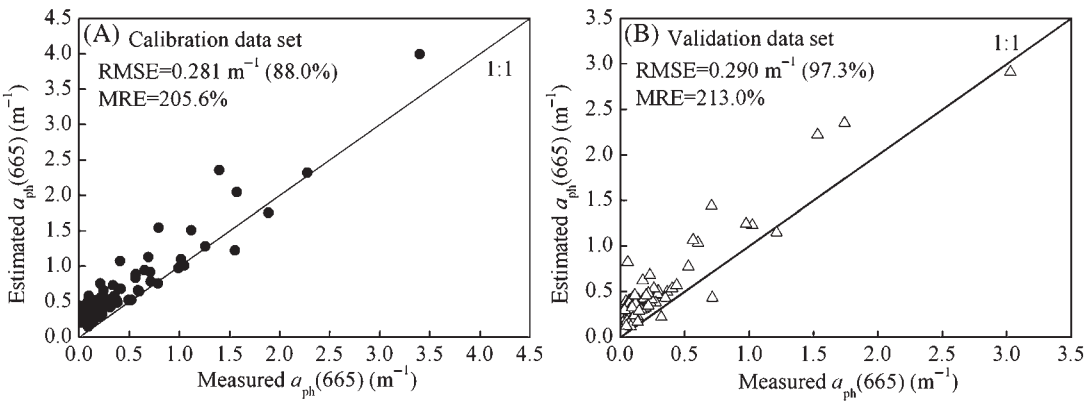

Fig. 11. Comparison of measured and estimated values using method of Simis *et al.* (2007) (equation (2)): (**A**) calibration data set, and (**B**) validation data set. The 88.0 and 97.3% in parentheses are the percentages of RMSE accounting for the mean $a_{ph}(665)$ for calibration and validation data sets, respectively.

accurate data on harmful blooms of toxic cyanobacteria in inland waters. Furthermore, remote sensing of phytoplankton absorption was the important input parameter of the primary production bio-optical model of Oliver *et al.* (Oliver *et al.*, 2004), and also presented information for pigment composition and phytoplankton size classes (Hoepffner and Sathyendranath, 1993; Ciotti *et al.*, 2002; Ciotti and Bricaud, 2006). Hoepffner and Sathyendranath (Hoepffner and Sathyendranath, 1993) demonstrated that pigment compositions can be derived from a hyperspectral $a_{ph}(\lambda)$ spectrum after applying a series of Gaussian bands reflecting absorption by phytoplankton pigments. Ciotti *et al.* (Ciotti *et al.*, 2002) and Ciotti and Bricaud (Ciotti and Bricaud, 2006) indicated that phytoplankton cell size can be implied from hyperspectral $a_{ph}(\lambda)$. Hirata *et al.* (Hirata *et al.*, 2008) developed a model linking phytoplankton absorption to phytoplankton size classes that use a single variable, the optical absorption by phytoplankton at 443 nm, $a_{ph}(443)$, which can be derived from the inversion of ocean color data.

CONCLUSIONS

Our results on the seasonal and spatial heterogeneity of the optically active substance concentrations and bio-optical properties (CDOM, phytoplankton absorption, Chl*a*-specific absorption and remote sensing reflectance) illustrate the complexity of the ecosystems of Lake Taihu, which should be considered for ecological purposes as well as for the interpretation of remote sensing data. Meteorology was the main factor driving the bio-optical properties of the water column in winter, whereas biological activity was another driving force in the spring–summer–autumn. The three-band model $[R_{rs}^{-1}(673) - R_{rs}^{-1}(698)] \times R_{rs}(731)$ of phytoplankton absorption $a_{ph}(665)$ was superior to the published semi-analytical model. Thus, the three-band model would improve PC estimation precision in inland waters. The three-band model allowed estimation of $a_{ph}(665)$ with the RMSE and MRE of 0.150 m^{-1} and 45.7%, respectively, whereas the published Simis *et al.* (Simis *et al.*, 2007) method had the RMSE and MRE of 0.290 m^{-1} and 213.0%, respectively, using an independent validation data set. The three-band and band-ratio models worked well in estimating phytoplankton absorption with simulated MERIS bands data with higher precision for the three-band model in Lake Taihu.

ACKNOWLEDGEMENTS

We especially thank S. Feng, X. Wang, Q. H. Zhao, and H. Zhang for their help with field sample collection.

FUNDING

This study was jointly supported by the Knowledge Innovation Project of the Chinese Academy of Sciences (KZCX2-YW-QN312) and the National Natural Science Foundation of China (Grant Nos 40825004, 40971252, 40730529).

REFERENCES

Allali, K., Bricaud, A. and Claustre, H. (1997) Spatial variations in the chlorophyll-specific absorption coefficients of phytoplankton and photosynthetically active pigments in the equatorial pacific. *J. Geophys. Res.*, **102**, 12413–12423.

Babin, M., Stramski, D., Ferrari, G. M. *et al.* (2003) Variations in the light absorption coefficients of phytoplankton, non-algal particles, and dissolved organic matter in coastal waters around Europe. *J. Geophys. Res.*, **108**, 1–20.

Binding, C. E., Jerome, J. H., Bukata, R. P. *et al.* (2008) Spectral absorption properties of dissolved and particulate matter in Lake Erie. *Remote Sens. Environ.*, **112**, 1702–1711.

Bricaud, A., Babin, M., Morel, A. *et al.* (1995) Variability in the chlorophyll-specific absorption coefficients of natural phytoplankton: analysis and parameterization. *J. Geophys. Res.*, **100**, 13321–13332.

Bricaud, A., Morel, A., Babin, M. *et al.* (1998) Variations of light absorption by suspended particles with chlorophyll a concentration in oceanic (case 1) waters: analysis and implications for bio-optical models. *J. Geophys. Res.*, **103**, 31033–31044.

Cao, W. X., Yang, Y. Z., Xu, X. Q. *et al.* (2003) Regional patterns of particulate spectral absorption in the Pearl River estuary. *Chinese Sci. Bull.*, **48**, 2344–2351.

Ciotti, A. M. and Bricaud, A. (2006) Retrievals of a size parameter for phytoplankton and spectral light absorption by colored detrital matter from water-leaving radiances at SeaWiFS channels in a continental shelf region off Brazil. *Limnol. Oceanogr. Meth.*, **4**, 237–253.

Ciotti, A. M., Lewis, M. R. and Cullen, J. J. (2002) Assessment of the relationships between dominant cell size in natural phytoplankton communities and spectral shape of the absorption coefficient. *Limnol. Oceanogr.*, **47**, 404–417.

Dall'Olmo, G. and Gitelson, A. A. (2005) Effect of bio-optical parameter variability on the remote estimation of chlorophyll-a concentration in turbid productive waters: experimental results. *Appl. Optics*, **44**, 412–422.

Dall'Olmo, G. and Gitelson, A. A. (2006) Effect of bio-optical parameter variability and uncertainties in reflectance measurements on the remote estimation of chlorophyll-a concentration in turbid productive waters: modeling results. *Appl. Optics*, **45**, 3577–3592.

Gitelson, A. A. (1992) The peak near 700nm on radiance spectra of algae and water: relationship of its magnitude and position with chlorophyll concentration. *Int. J. Remote Sens.*, **13**, 3367–3373.

Giardino, C., Brando, V. E., Dekker, A. G. *et al.* (2007) Assessment of water quality in Lake Garda (Italy) using Hyperion. *Remote Sens. Environ.*, **109**, 183–195.

Gitelson, A. A., Schalles, J. F. and Hladik, C. M. (2007) Remote chlorophyll-a retrieval in turbid, productive estuaries: Chesapeake Bay case study. *Remote Sens. Environ.*, **109**, 464–472.

Gitelson, A. A., Dall'Olmo, G., Moses, W. *et al*. (2008) A simple semi-analytical model for remote estimation of chlorophyll-a in turbid waters: validation. *Remote Sens. Environ.*, **112**, 3582–3593.

Gons, H. J. (1999) Optical teledetection of chlorophyll a in turbid inland waters. *Environ. Sci. Technol.*, **3**, 1127–1132.

Gons, H. J., Rijkeboer, M. and Ruddick, K. G. (2005) Effect of a waveband shift on chlorophyll retrieval from MERIS imagery of inland and coastal waters. *J. Plankton Res.*, **27**, 125–127.

Gons, H. J., Auer, M. T. and Effler, S. W. (2008) MERIS satellite chlorophyll mapping of oligotrophic and eutrophic waters in the Laurentian Great Lakes. *Remote Sens. Environ.*, **112**, 4098–4106.

Gordon, H. R., Brown, O. B. and Jacobs, M. M. (1975) Computed relationships between the inherent and apparent optical properties of a flat homogeneous ocean. *Appl. Optics*, **14**, 417–427.

Hirata, T., Aiken, J., Hardman-Mountford, N. *et al*. (2008) An absorption model to determine phytoplankton size classes from satellite ocean colour. *Remote Sens. Environ.*, **112**, 3153–3159.

Hoepffner, N. and Sathyendranath, S. (1993) Determination of the major groups of phytoplankton pigments from the absorption spectra of total particulate matter. *J. Geophys. Res.*, **98**, 22789–22803.

Kirk, J. T. O. (1994) *Light and Photosynthesis in Aquatic Ecosystems*. Cambridge University Press, Cambridge, UK.

Kutser, T., Metsamaa, L., Strömbeck, N. *et al*. (2006) Monitoring cyanobacterial blooms by satellite remote sensing. *Estuarine Coastal Shelf Sci.*, **67**, 303–312.

Laurion, I., Ventura, M., Catalan, J. *et al*. (2000) Attenuation of ultraviolet radiation in mountain lakes: factors controlling the among- and within-lake variability. *Limnol. Oceanogr.*, **45**, 1274–1288.

Li, Y. L., Zhang, Y. L., Li, J. S. *et al*. (2008) Comparison of chlorophyll a concentration estimation in Taihu Lake using different methods. *Environ. Sci.*, **20**, 153–159. (In Chinese with English abstract).

Lutz, V. A., Sathyendranath, S. and Head, E. J. H. (1996) Absorption coefficient of phytoplankton: regional variations in the North Atlantic. *Mar. Ecol. Prog. Ser.*, **135**, 197–213.

Millán-Núñez, E., Sierackib, M. E., Millán-Núñez, R. *et al*. (2004) Specific absorption coefficient and phytoplankton biomass in the southern region of the California Current. *Deep-Sea Res. II*, **51**, 817–826.

Moses, W. J., Gitelson, A. A., Berdnikov, S. *et al*. (2009) Satellite estimation of chlorophyll-a concentration using the red and NIR bands of MERIS—the Azov Sea case study. *IEEE Geosci. Remote Sci.*, **6**, 845–849.

Oliver, M. J., Schofield, O., Bergmann, T. *et al*. (2004) Deriving in situ phytoplankton absorption for bio-optical productivity models in turbid waters. *J. Geophys. Res.*, **109**, C07S11.

Prieur, L. and Sathyendranath, S. (1981) An optical classification of costal and oceanic waters based on the specific spectral absorption curves of phytoplankton pigments, dissolved organic matter, and other particulate materials. *Limnol. Oceanogr.*, **26**, 671–689.

Randolph, K., Wilson, J., Tedesco, L. *et al*. (2008) Hyperspectral remote sensing of cyanobacteria in turbid productive water using optically active pigments, chlorophyll a and phycocyanin. *Remote Sens. Environ.*, **112**, 4009–4019.

Ruiz-Verdú, A., Simis, S. G. H., de Hoyos, C. *et al*. (2008) An evaluation of algorithms for the remote sensing of cyanobacterial biomass. *Remote Sens. Environ.*, **112**, 3996–4008.

Sasaki, H., Saitoh, S. I. and Kishino, M. (2001) Bio-optical properties of seawater in the western subarctic Gyre and Alaskan Gyre in the subarctic north Pacific and the southern Bering Sea. *J. Oceanogr.*, **57**, 275–284.

Simis, S. G. H., Peters, S. W. M. and Gons, H. J. (2005) Remote sensing of the cyanobacterial pigment phycocyanin in turbid inland water. *Limnol. Oceanogr.*, **50**, 237–245.

Simis, S. G. H., Ruiz-Verdú, A., Domínguez-Gómez, J. A. *et al*. (2007) Influence of phytoplankton pigment composition on remote sensing of cyanobacterial biomass. *Remote Sens. Environ.*, **106**, 414–427.

Sosik, H. M. and Mitchell, B. G. (1995) Light absorption by phytoplankton, photosynthetic pigments and detritus in the California Current System. *Deep-Sea Res. I*, **42**, 1717–1748.

Stedmon, C. A., Markager, S. and Kaas, H. (2000) Optical properties and signatures of chromophoric dissolved organic matter (CDOM) in Danish coastal waters. *Estuarine Coastal Shelf Sci.*, **51**, 267–278.

Stuart, V., Sathyendranath, S., Head, E. J. H. *et al*. (2000) Bio-optical characteristics of diatom and prymnesiophyte populations in the Labrador Sea. *Mar. Ecol. Prog Ser.*, **201**, 91–106.

Suzuki, K., Kishino, M., Sasaoka, K. *et al*. (1998) Chlorophyll-specific absorption coefficients and pigments of phytoplankton off Sanriku, Northwestern North Pacific. *J. Oceanogr.*, **54**, 517–526.

Tang, J. W., Tiang, G. L., Wang, X. Y. *et al*. (2004) The methods of water spectra measuring and analysis I: above-water method. *J. Remote Sens.*, **8**, 37–44. (In Chinese with English abstract).

Vähätalo, A. V., Wetzel, R. G. and Paerl, H. W. (2005) Light absorption by phytoplankton and chromophoric dissolved organic matter in the drainage basin and estuary of the Neuse River, North Carolina (USA). *Freshwater Biol.*, **50**, 477–493.

Xu, J. P., Li, F., Zhang, B. *et al*. (2009) Estimation of chlorophyll-a concentration using field spectral data: a case study in inland Case-II waters, North China. *Environ. Monit. Assess.*, **158**, 105–116.

Zhang, Y. L., Zhang, B., Wang, X. *et al*. (2007) A study of absorption characteristics of chromophoric dissolved organic matter and particles in Lake Taihu, China. *Hydrobiologia*, **592**, 105–120.

Zhang, Y. L., Liu, M. L., Qin, B. Q. *et al*. (2009a) Modeling remote-sensing reflectance and retrieving chlorophyll-a concentration in extremely turbid Case-2 waters (Lake Taihu, China). *IEEE T. Geosci. Remote*, **47**, 1937–1948.

Zhang, Y. L., Liu, M. L., van Dijk, M. A. *et al*. (2009b) Measured and numerically partitioned phytoplankton spectral absorption coefficient in inland waters. *J. Plankton Res.*, **31**, 311–323.

Zimba, P. V. and Gitelson, A. A. (2006) Remote estimation of chlorophyll concentration in hyper-eutrophic aquatic systems: model tuning and accuracy optimization. *Aquaculture*, **256**, 272–286.